

# **Final Report**

## **Site-Specific Tsunami Modeling at the Jordan Cove LNG Facility Coos County, Oregon**

**Prepared by**

**Yinglong Joseph Zhang, Ph.D.**

**Center for Coastal Margin Observation & Prediction (CMOP)  
Oregon Health & Science University**

**September 25, 2008**

### **Summary**

The proposed Liquefied Natural Gas (LNG) Terminal site is located east of Henderson Marsh on the North Spit in Coos County, Oregon; across the Coos River shipping channel from the airport in North Bend (Fig. 1). The potential tsunami hazard near the proposed LNG Terminal was studied using a state-of-the-art hydrodynamic model and three earthquake scenarios for this region. Maximum tsunami wave inundations and velocities around the project site were calculated. Using the current suite of earthquake scenarios, the maximum calculated tsunami inundation at the site is about elevation 21 ft (NAVD88).

### **Project Overview**

The purpose of this investigation was to conduct site-specific tsunami modeling for the proposed Jordan Cove Energy LNG Terminal in Coos County, Oregon, using Oregon Health & Science University's (OHSU) SELFE hydrodynamic model (Zhang and Baptista, 2008a). The objective of the modeling study was to update existing tsunami studies of the area, last done by Oregon Department of Geology and Mineral Industries (DOGAMI) about eight years ago using a combination of numerical model and field estimates (Priest, private communication), and provide criteria for the design of mitigation measures to limit the impact of a tsunami on the site and terminal.

Assuming an accurate topographic model of the site and surroundings, the most important issue in site-specific studies like this is the choice of geologically relevant earthquake or source models. OHSU, in collaboration with DOGAMI and others, has studied tsunami hazards at Cannon Beach, OR, using the SELFE model, and source model mostly from a geological model based on the Northern Cascadia Subduction Zone. For the current project, a Southern Cascadia source is of most relevance. Unfortunately, at the time of this investigation the Southern Cascadia source is still under development, and only a couple of scenarios, based on geological evidence (e.g., offshore turbidite data), have been proposed (see below). Therefore, we have

adopted a hybrid approach using a few source models that we believe are most likely to impact Coos Bay and the project site.

## **Method**

The existing topography around the site has been surveyed using 1-foot resolution LIDAR technology in February 2008, based on which a Digital Elevation Model (DEM) was constructed. Development of the LNG Terminal will include the following major landscape modifications: (1) dredging for an access channel and slip in the southern part of the site with docks on the north and east sides; and (2) regrading the northern part of the site (up to the railway) and building a berm around the proposed location of the two LNG tanks. The proposed site landscape can be seen in Fig. 2.

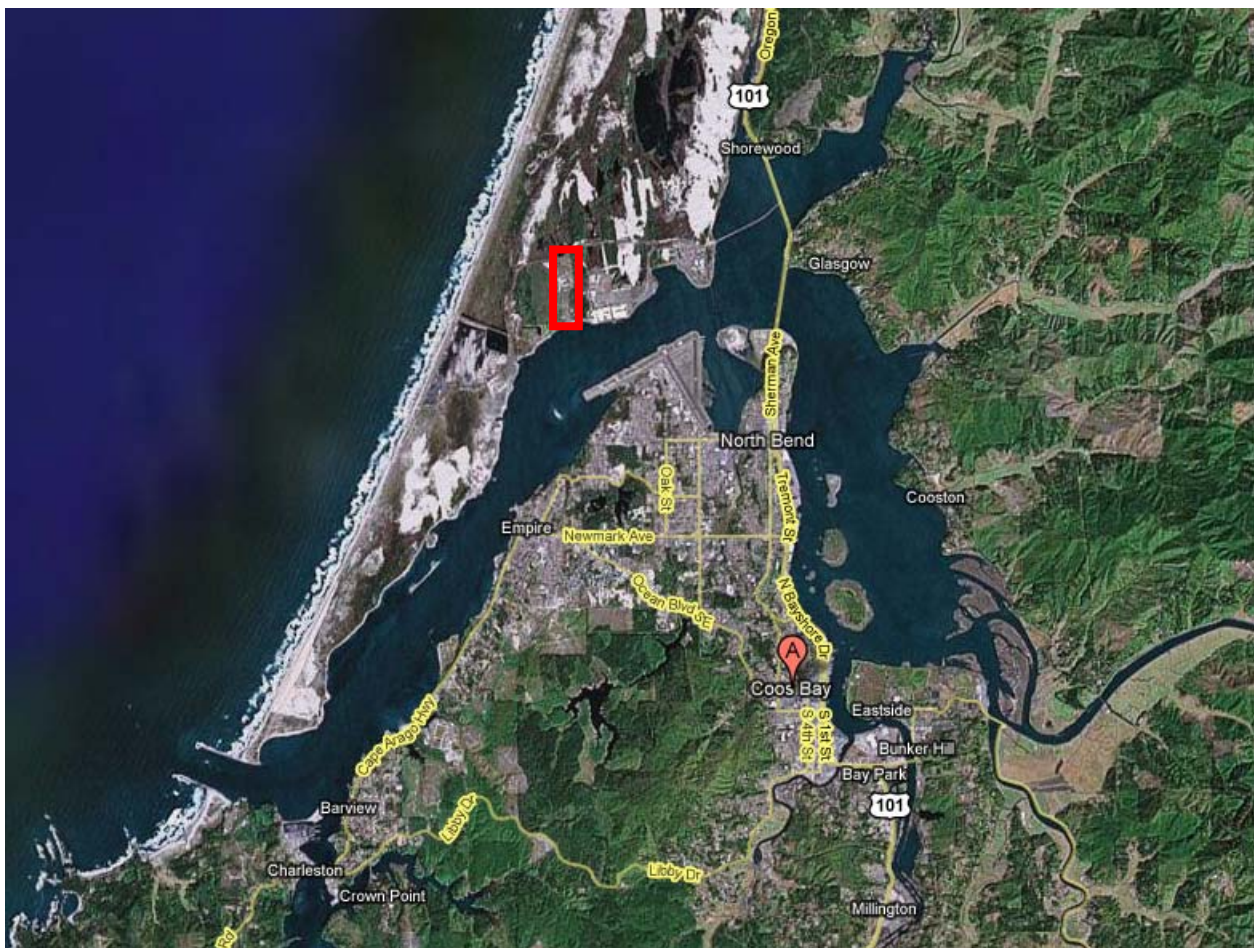


Figure 1 Google map of Coos Bay, OR. Red box indicates approximate location of project site.

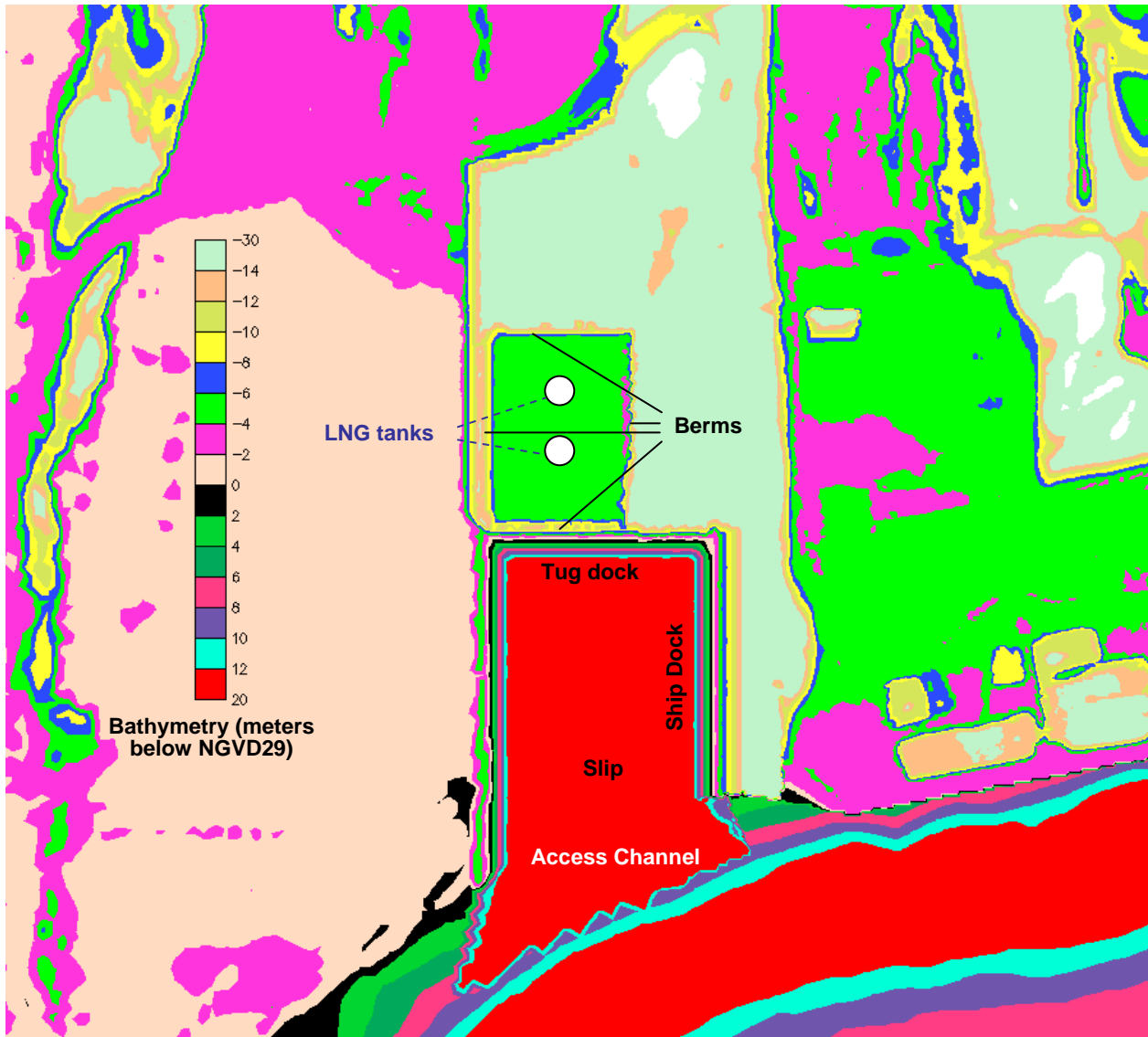


Figure 2 Proposed landscape for the LNG terminal. Negative values correspond to dry land.

The proposed changes to the existing topography, as outlined in the previous paragraph, were then incorporated into a new DEM as the “modified” landscape.

The hydrodynamic model used in this project was SELFE (Zhang and Baptista, 2008a). Originally developed at OHSU as a three-dimensional (3D), *unstructured*-grid, baroclinic circulation model, SELFE has been rigorously benchmarked for tsunami test cases (Zhang and Baptista, 2008b), and successfully applied to document past tsunamis in Cannon Beach, OR (Priest, et al., 2008). The model uses a semi-implicit finite-element/finite-volume approach, coupled with Eulerian-Lagrangian method for advection, and is very efficient, accurate, and robust for a variety of estuary and coastal applications. The use of unstructured grids in the model allows maximum flexibility in resolving complex geometry and bathymetry commonly found in the bays and estuaries. Although the model is fully 3D, for tsunami applications the quasi-2D configuration of the model is typically used, for maximum efficiency and more

importantly, because some 3D aspects of tsunamis are not well understood (Zhang and Baptista, 2008b). However, it would be a minor task to apply the model in its full 3D configuration if warranted in the future.

The first source model we used came from DOGAMI's historical model for northern and southern CSZ. We chose one of the largest scenarios (1A) for this region (Myers, 1998) that was used in the DOGAMI mapping effort published in 2002. The second and third source models were the first two new southern CSZ scenarios from DOGAMI's new project in this region; the difference between the two models is the fault slip distribution (symmetric vs. seaward skewed). Two earthquake return intervals (related to the magnitude of the earthquake), 280 and 579 years, were used to represent average and worst-case scenarios, respectively, based on preliminary analysis of the turbidite data (Chris Goldfinger, private communication). Note that the return intervals are substantial smaller in this region as compared with the northern CSZ, indicating more frequent but smaller earthquakes in the southern CSZ. For tsunami wave simulation, all source models were applied to two landscapes: existing and modified topography.

An unstructured computational grid, with 314,889 nodes and 620,195 triangular elements, was generated to resolve major features in Coos Bay and around the proposed site (Fig. 3). Typical horizontal resolution around the site is ~6m. A 2-hour simulation was carried out for each scenario and landscape, which took 13 hours CPU time on an AMD Opteron 2.2GHz processor. Sensitivity test results indicated that wave activity continued after 2 hours with much reduced intensity (not shown here). The earthquake was modeled as being instantaneous (as customary in most tsunami simulations), resulting in an initial surface slope that mirrors the seabed deformation and drives the subsequent fluid motion. Tides were not explicitly modeled in the simulation; the vertical datum used in the simulations was NGVD29, which corresponds to the most probable event (i.e., average tidal datum). Per project specification, all results presented below have been converted from NGVD29 to NAVD88.

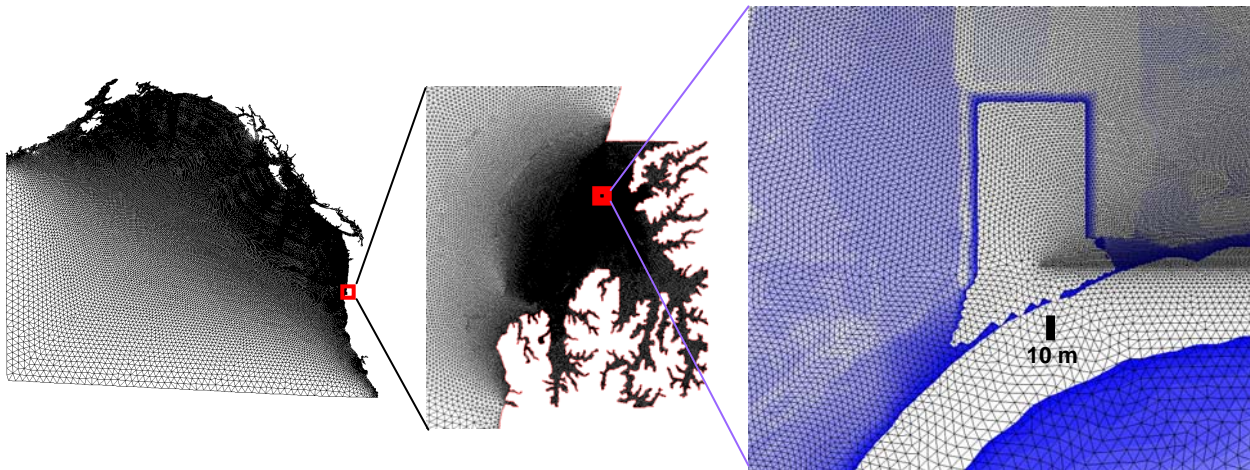


Figure 3 Grids (entire grid, Coos Bay portion, and zoom-in of the project site); modified landscape only.

## **Results and Discussion**

Ten runs have been completed for this project, corresponding to different source models on landscapes (Table 1). The elevation results presented in this section all referenced the NAVD88 datum.

**Table 1. Description of Simulations**

<b>Run ID</b>	<b>Source Model</b>	<b>Return Interval (years)</b>	<b>Estimated Slip (m)</b>	<b>Landscape</b>
RUN22	Symmetric (f1p2s2)	280	8	Existing
RUN23	Symmetric (f1p2s2)	280	8	Modified
RUN24	Symmetric (f1p2s2)	579	17	Existing
RUN25	Symmetric (f1p2s2)	579	17	Modified
RUN26	1A	450	15-20	Existing
RUN27	1A	450	15-20	Modified
RUN28	Seaward skewed (f1p2s23)	280	8	Existing
RUN29	Seaward skewed (f1p2s23)	280	8	Modified
RUN30	Seaward skewed (f1p2s23)	579	17	Existing
RUN31	Seaward skewed (f1p2s23)	579	17	Modified

We first present some typical inundation sequences from the largest earthquake scenario considered (RUN30 and RUN31) (Fig. 4). The inundations onto the two landscapes are largely coherent: the first wave arrives at the beach approximately 20 minutes after the earthquake, at the project site ~5 minutes later; the maximum inundation near the site occurs ~40 minutes after the earthquake (see below), and the second tsunami wave arrives ~55 minutes after the earthquake, and compounds on the retreating water (from the first wave) in some areas (not shown). The third wave arrives ~72 minutes after the earthquake, but is substantially smaller than the first two (not shown). There are small variations in these times among different scenarios, but the sequences are largely consistent with these two runs.

The first wave actually consists of two separate waves, one from the overland flow over the sand dunes and the other propagating inward from the entrance of the Coos Bay along the shipping channel (cf. Fig. 1). The “dune wave” reaches the site first due to the shorter traveling distance from the beach. Stacking of waves occurs as the two first waves collide in the shipping channel, resulting in the maximum inundation near the project site ~15 minutes after the arrival of the dune waves. The modified landscape causes slightly smaller waves and less water to spill into the Henderson Marsh (Fig. 4). The slip also has caused some localized wave patterns as expected (Fig. 8).

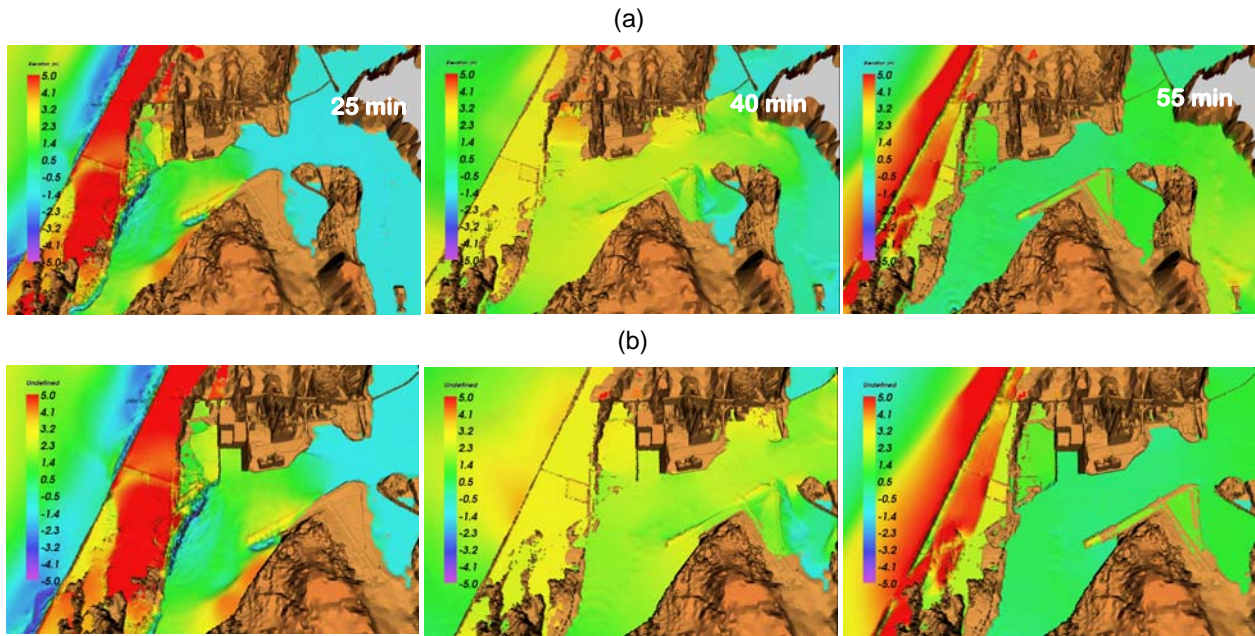


Fig. 4 Inundation sequences for (a) RUN30 and (b) RUN31. The first column corresponds to the arrival of the first wave (via sand dunes) near the site, the second column corresponds approximately to the time of maximum inundation around the project site (due to stacking of two waves) and the third column corresponds to the arrival of second (smaller) wave. The tsunami time for each column is indicated in (a).

The maximum water elevations and velocities are two important parameters in hazard assessment. Fig. 5 shows the maximum elevations for all scenarios near the site. The maximum inundations (i.e., the shoreline position corresponding to the local maximum wave) are shown in Fig. 6; for contrasting purpose, the results on the original landscape are also shown in these figures.

In the smallest scenario (RUN22 and 23) the overland flow from the dunes does not reach the project site, and the inundation there is entirely due to the waves coming in from the entrance of Coos Bay (Fig. 5). In the second smallest scenario (RUN28 and 29), the overland flow barely crosses over into the shipping channel, where the maximum wave height is  $\sim 2$  m. In the three larger scenarios (1A and two new southern CSZ cases with 579-year return interval), the dominant waves come from the dunes, which reach  $>10$  m height in the dunes in 1A and the asymmetric case (RUN27 and 31). The “dune waves” also exhibit complex run-up patterns due to topographical changes. In these scenarios, the wave height is 5-6 m inside the slip (Fig. 5b). In all scenarios, the original landscape causes larger waves and slightly more inundation into the Henderson Marsh; the presence of the slip has “absorbed” some waves.

The maximum inundation patterns are consistent with the maximum elevations (Fig. 6). The three larger scenarios cause larger inundation than the two smaller scenarios. As a point of reference, only in the asymmetric scenario (RUN28 and 29) does the airport runway south of the site remain dry. The 1A scenario (RUN27) inundates more to the north of the project site, but the symmetric scenario (RUN25) inundates more to the east of the site (Fig. 6). Except for several stretches of the sand barriers and isolated high-elevation spots, the region to the west of the site is under water in all three larger scenarios (Fig. 6). None of the scenario waves overtops the

berm or dune north and west of the site at elevation 55 feet, and the highest calculated elevation near the berm is approximately 18 feet on the west side and 21 feet on the south side of the berm.

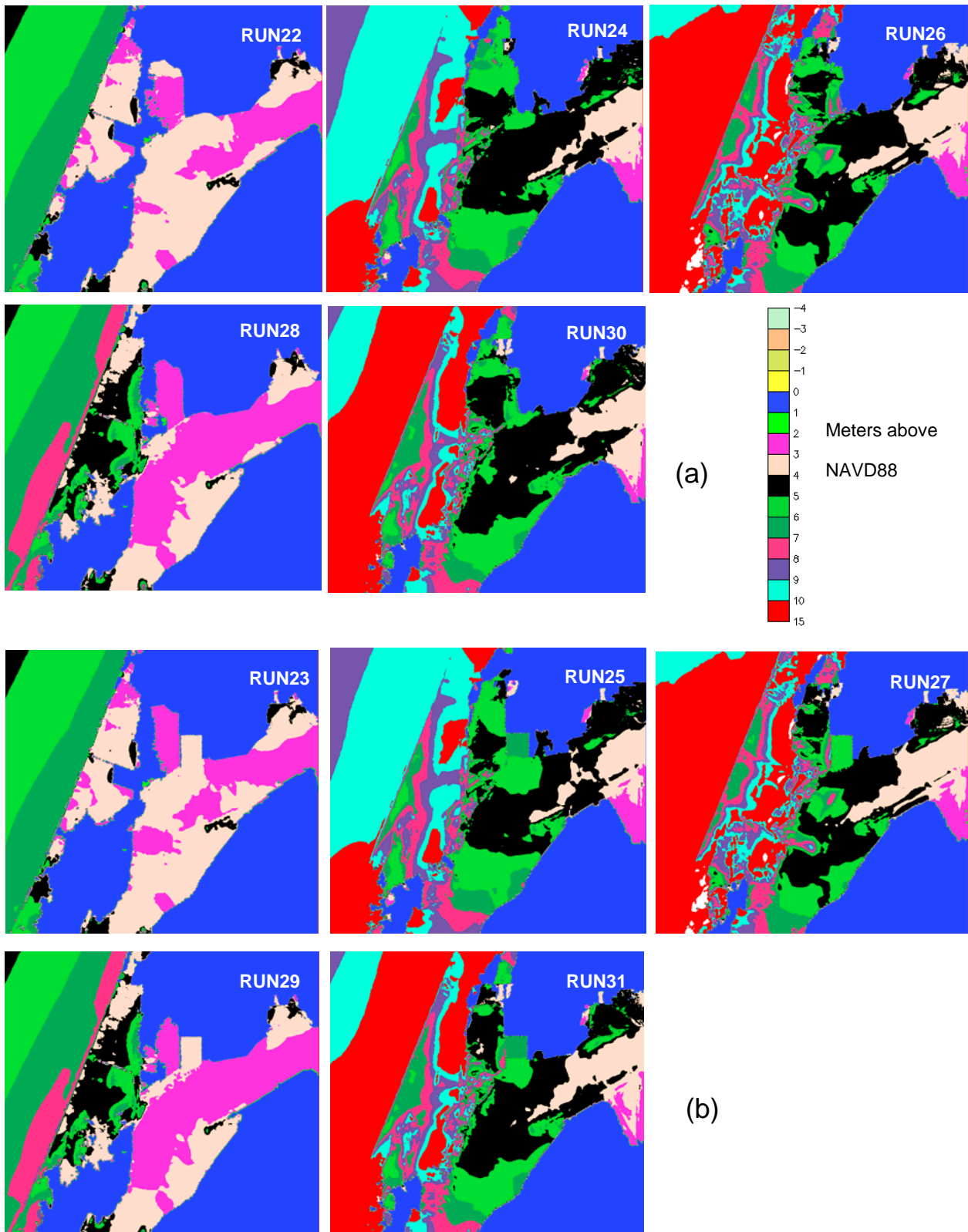


Fig. 5 Maximum elevations for each scenario on the (a) original and (b) modified landscapes. RUN 22, 23, 28 and 29 represent smaller scenarios.

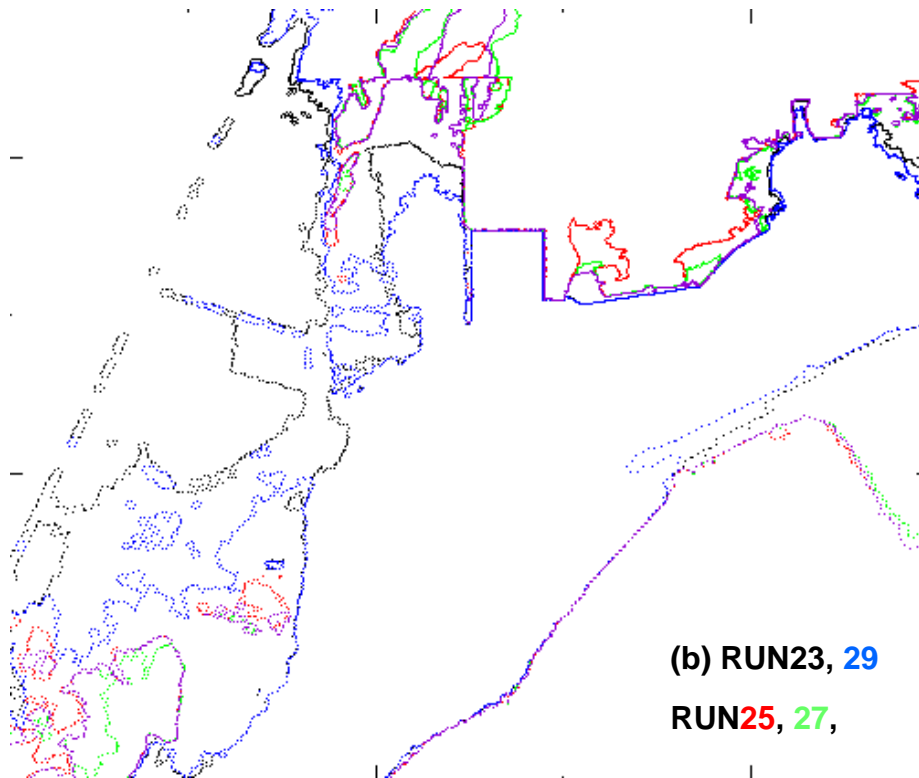
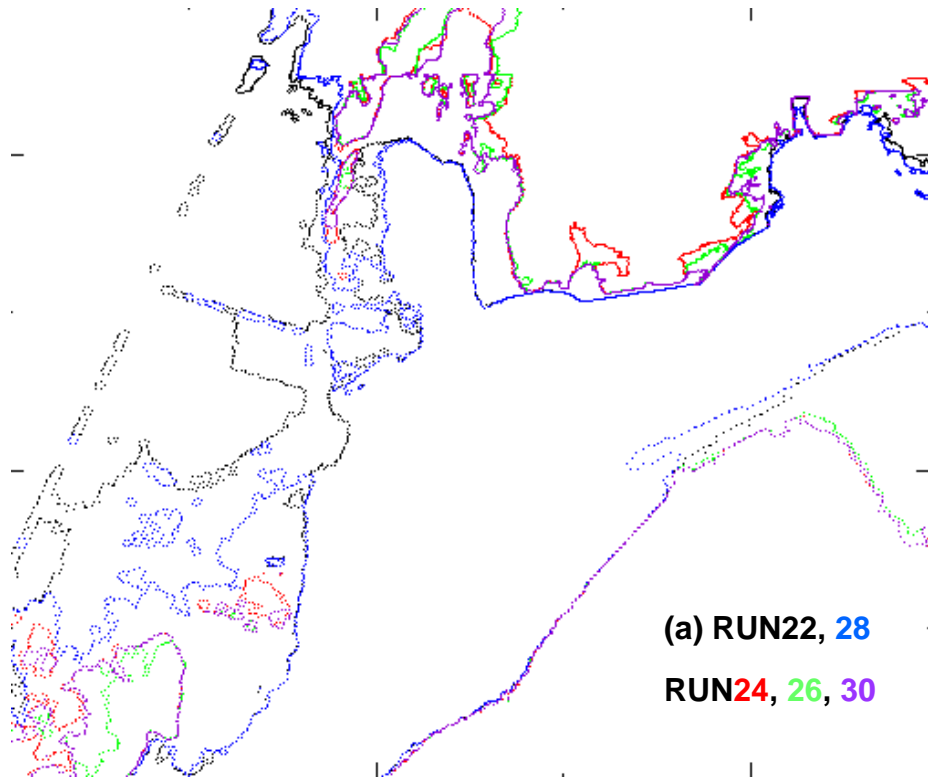


Fig. 6 Maximum inundation lines for each scenarios on (a) original and (b) modified landscapes. RUN22, 23, 28 and 29 represent smaller scenarios.

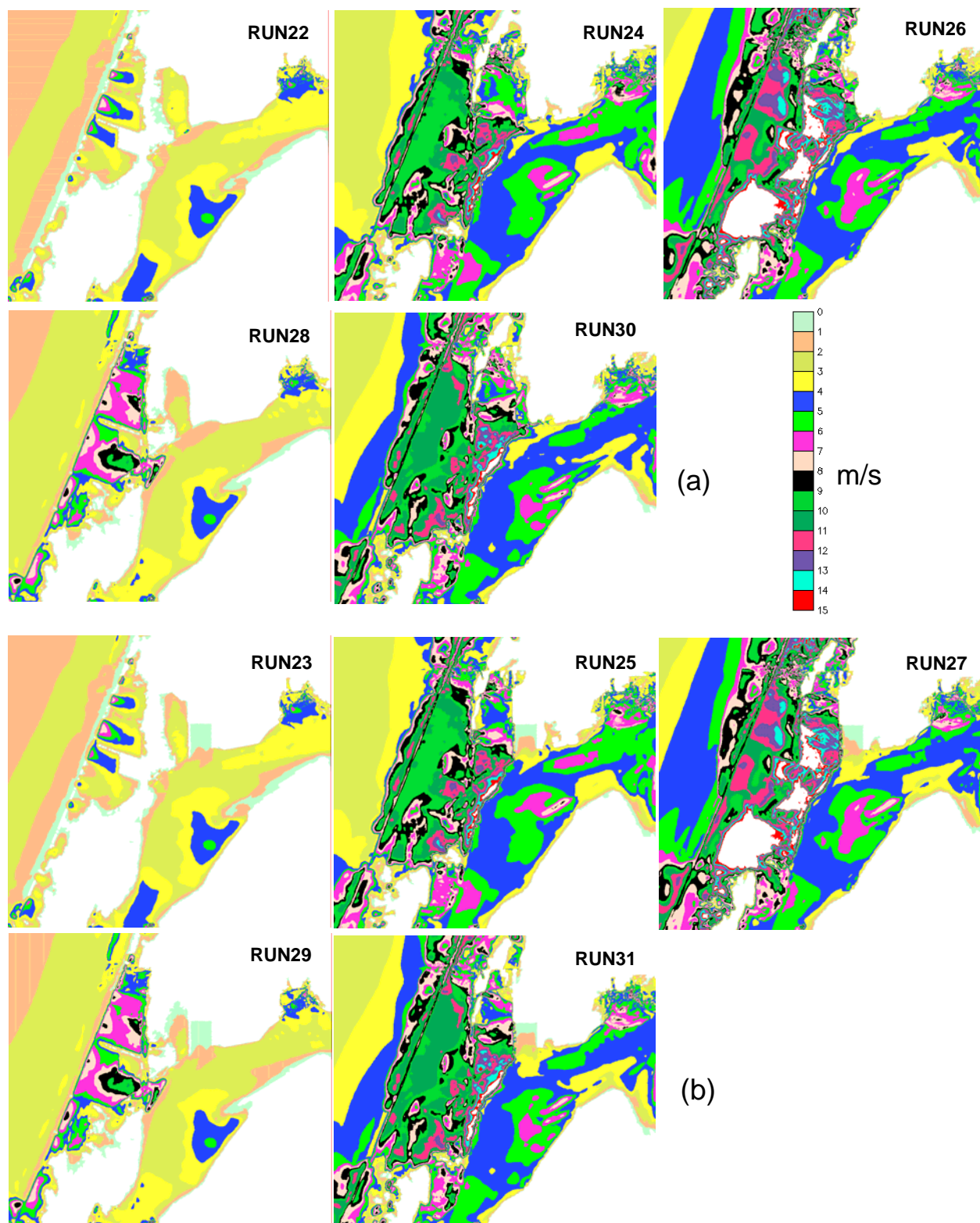


Fig. 7 Maximum velocities for each scenario on (a) original and (b) modified landscapes.

The calculated maximum velocities for all scenarios are shown in Fig. 7. While velocities reach 2-3 m/s in the two smaller scenarios (RUN22, 23, 28, and 29) in the shipping channel, the maximum velocity reaches 4-5 m/s or higher in the larger scenarios. Fastest flow ( $>10$  m/s) occurs over the sand dunes in the larger scenarios, and the maximum flow ( $\sim 15$  m/s) occurs to the west and southwest of the slip in the asymmetric case (RUN30 and 31) (Fig. 7). The flow slows down considerably when it reaches the slip mainly due to its west bank that effectively blocks most of the incoming wave from the west; as a result, the waves in the slip come in primarily from the shipping channel, and the maximum flow is only  $\sim 2$  m/s. Again, the berm remains above the maximum inundation line in all scenarios.

Finally, to assist the scouring and structural analysis of the docks, time history of the elevations and velocities at four locations in the slip (north, west and two in the east) is shown in Fig. 8. Only the results on the modified landscape are shown because these four locations remain dry throughout the tsunami event on the existing landscape.

Fig. 8b shows interesting wave compounding effects during the first incoming wave. While the “dune” wave reaches the harbor 25 minutes after the earthquake, the highest wave results from the collision between the dune wave and the wave propagating in from the entrance of Coos Bay along the shipping channel, and reaches the harbor  $\sim 10$ -15 minutes later. The wave height is  $\sim 6$  m at all four slip locations in the larger scenarios, and  $\sim 4$  m in the smaller scenarios (Fig. 8b). The second and later waves have significantly smaller amplitudes, but oscillation persists after 2 hours.

There is considerable variation of velocities at the four slip locations (Fig. 8c,d). The highest velocity occurs during the first wave. The east-west velocity is generally smaller than the north-south velocity, indicating the primary wave direction is from the south to north. The wave slows down as it travels from the south to north (Fig. 8c,d). Therefore, the west and east docks will experience significant shear, while the north dock will mainly experience head-on impact. The asymmetric scenario (RUN31) causes the largest north-south flow ( $\sim 1$  m/s), while the 1A scenario causes the largest east-west flow ( $\sim 0.7$  m/s). The times of maximum velocity vary by a few minutes among different scenarios, and the larger scenarios tend to have multiple peak flows, as a result of the two separate first waves (e.g., RUN31 in Fig. 8d).

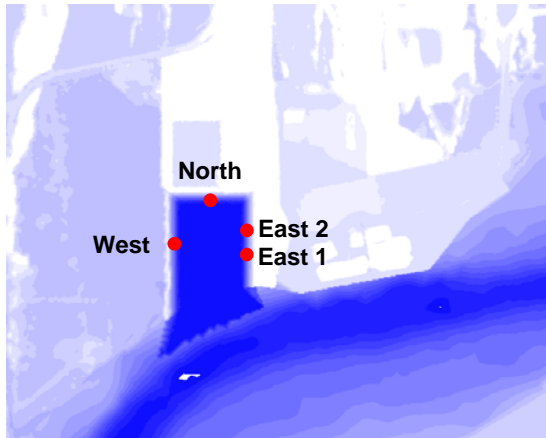
### **Limitations of the Current Approach**

The analysis presented in this report was conducted with a subset of the estimated 25+ southern CSZ scenarios, and thus the assessment may be biased one way or another. A comprehensive approach as we have used for the northern CSZ study is certainly more desirable and will become possible as soon as the complete southern CSZ scenarios are developed.

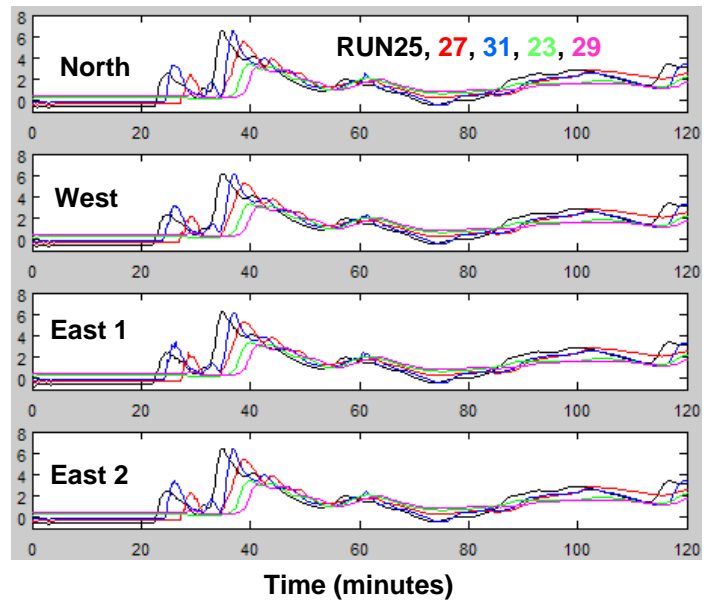
Tsunamis of remote origins (tele-tsunamis) may impact this region, but the effects are expected to be smaller compared with the local earthquakes. For example, the 1964 Prince Williams Sound earthquake only generated about 3 feet of water in the City of Cannon Beach as compared with depths of 10 feet or deeper in the average local scenario (Priest, et al., 2008).

The hydrodynamic model used in this project assumes the structures (jetties, barriers, dunes, etc.) are immobile throughout the tsunami event, which may not hold true especially during larger earthquakes. As a first estimate, the impact of tsunami wave forces on these structures can be analyzed using the wave surface elevations and flow velocities calculated here.

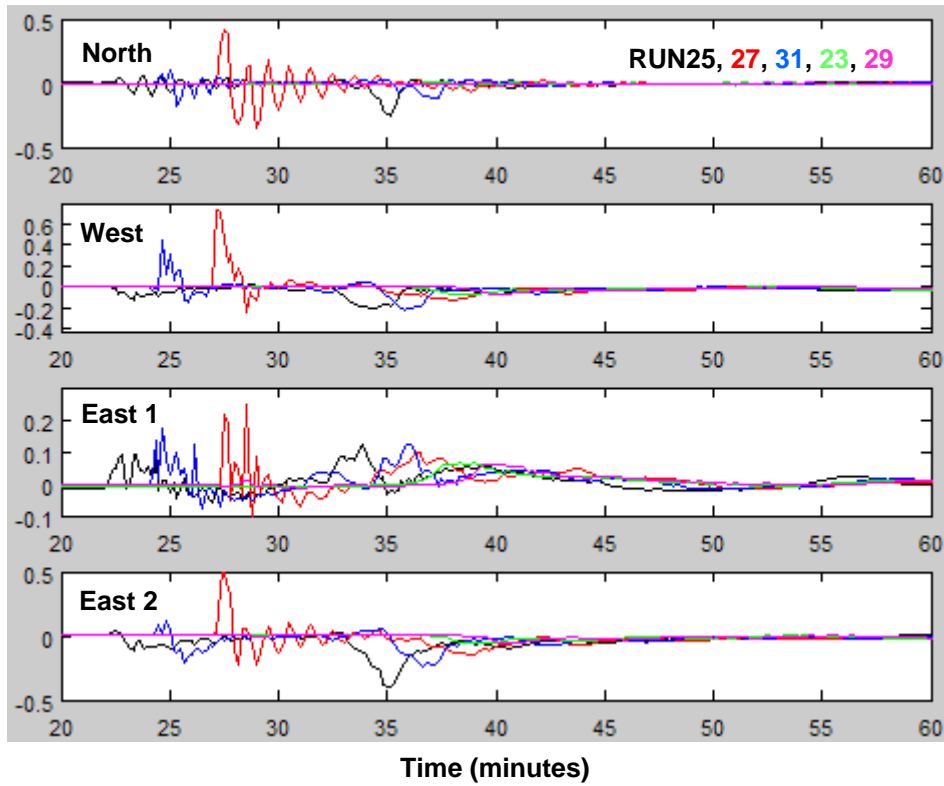
(a)



(b) Elevation (meters above NAVD88)



(c) U-velocity (m/s)



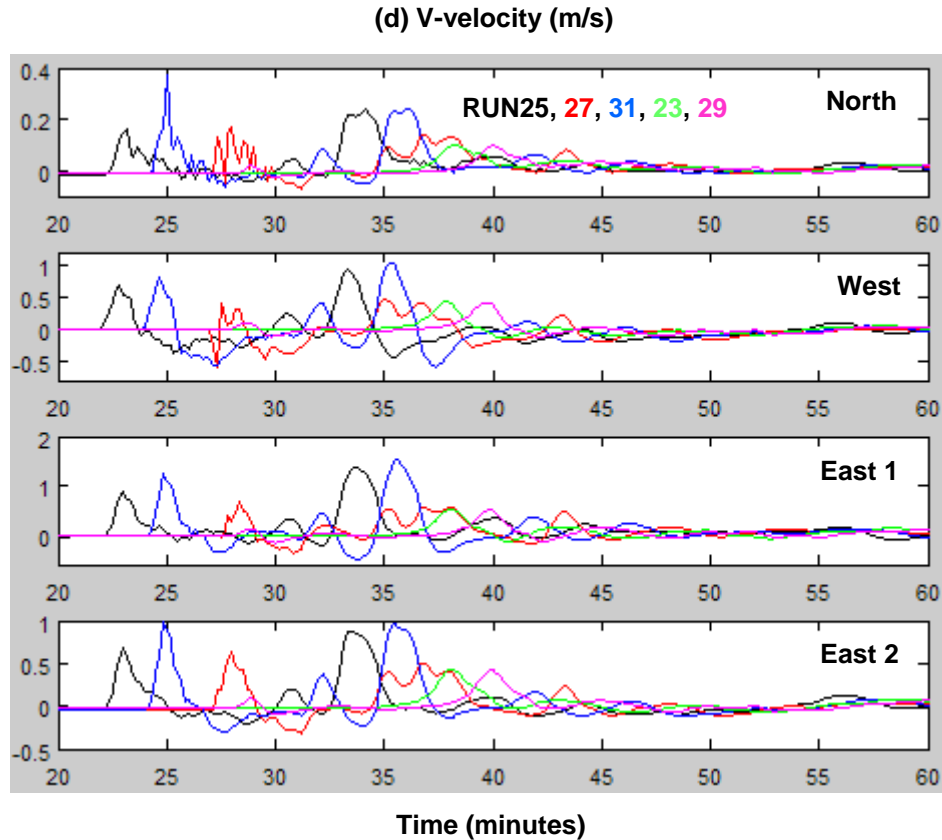


Fig. 8 (a) Four locations within the proposed slip where time history of elevation and velocity are extracted; (b) time history of elevations at the four slip locations; (c) time history of u-velocity (positive eastward) at the four slip locations; (c) time history of v-velocity (positive northward) at the four slip locations. Note that in (c) and (d) only period with significant velocity is shown for clarity.

## **References**

Myers, E.P., 1998, Physical and numerical analysis of long wave modeling for tsunamis and tides. Ph.D. dissertation, Environmental Science and Engineering, Oregon Graduate Institute of Science and Technology: 273 pp.

Priest, G.R., Goldfinger, C., Wang, K., Witter, R., Zhang, Y.L. and Baptista, A.M., 2008, Tsunami hazard assessment for cascadia subduction zone earthquakes: Cannon Beach, Oregon. Internal report of Department of Geology and Mineral Industries, Oregon (under review).

Zhang, Y.L., and Baptista, A.M., 2008a, SELFE: A semi-implicit Eulerian-Lagrangian finite-element model for cross-scale ocean circulation. *Ocean Modelling*, 21(3-4), 71-96.

Zhang, Y.L., and Baptista, A.M., (2008b), Benchmarking a new finite-element tsunami model on unstructured grids. *Pure and Applied Geophysics: Topical issue on Tsunamis* (accepted).